



HAL
open science

A solution- and gas-phase study of uranyl hydroxamato complexes

Vladimir Sladkov, Mingjian He, Pawel Jewula, Marie-José Penouilh, Stéphane Brandès, Christine Stern, Jean-Claude Chambron, Michel Meyer

► **To cite this version:**

Vladimir Sladkov, Mingjian He, Pawel Jewula, Marie-José Penouilh, Stéphane Brandès, et al.. A solution- and gas-phase study of uranyl hydroxamato complexes. *Journal of Radioanalytical and Nuclear Chemistry*, 2018, 318 (1), pp.259-266. 10.1007/s10967-018-6019-6 . hal-01998942

HAL Id: hal-01998942

<https://hal.science/hal-01998942>

Submitted on 21 Dec 2021

HAL is a multi-disciplinary open access archive for the deposit and dissemination of scientific research documents, whether they are published or not. The documents may come from teaching and research institutions in France or abroad, or from public or private research centers.

L'archive ouverte pluridisciplinaire **HAL**, est destinée au dépôt et à la diffusion de documents scientifiques de niveau recherche, publiés ou non, émanant des établissements d'enseignement et de recherche français ou étrangers, des laboratoires publics ou privés.

A Solution and Gas-Phase Study of Uranyl Hydroxamate Complexes

Vladimir Sladkov^{1*}, Mingjian He¹, Pawel Jewula², Marie-José Penouilh², Stéphane Brandès²,
Christine Stern², Jean-Claude Chambron², Michel Meyer²

¹ *Institut de Physique Nucléaire d'Orsay (IPNO), UMR 8608, CNRS-IN2P3, Université Paris Sud, 15 rue George Clemenceau, 91406 Orsay Cedex, France*

² *Institut de Chimie Moléculaire de l'Université de Bourgogne (ICMUB), UMR 6302, CNRS, Université Bourgogne–Franche-Comté, 9 avenue Alain Savary, BP 47870, 21078 Dijon Cedex, France*

Abstract

This study compares the binding properties towards the uranyl cation of three hydroxamates derived from benzohydroxamic acid (BHAH), *N*-methylacetohydroxamic acid (NMAH) and 1-hydroxypiperidine-2-one (PIPOH), as models of the binding sites found in natural chelators that could be involved in the mobilization of uranyl in the vicinity of abandoned mines. Solution speciation studies of the UO_2^{2+} /BHAH system by affinity capillary electrophoresis allowed to estimate stability constants for both ML ($\log K_{110} = 7.4(1)$) and ML_2 ($\log K_{120} = 7.0(1)$) species in aqueous media (0.1 M (H,Na)ClO₄, 25 °C), which lie in-between those reported by us elsewhere for NMA^- and PIPO^- . By contrast, gas phase studies demonstrate that one of the U=O bonds can be activated in the NMA^- and PIPO^- complexes, whereas this is not the case for the BHA^- complex.

Keywords

Benzohydroxamic acid, cyclic hydroxamic acid, U=O bond activation, speciation, capillary electrophoresis

Introduction

Uranium mines have been exploited in France from 1945–2001 [1]. During this period, 5.2×10^7 tons of ore have been extracted together with 2×10^8 tons of barren rocks to recover 8×10^4 tons of uranium by lixiviation, either *in situ* (static lixiviation), or in factories (dynamic lixiviation). Barren rocks and residues from static lixiviation have been used for conditioning and warranting the safety of old mining sites. These materials are considered long-lived, weakly or very weakly radioactive (10^3 – 10^5 Bq kg⁻¹). Before pitchblende (UO₂) deposits were discovered in the Limousin area, the first mines exploited contained ores of the autunite family (M₂(UO₂)₂(PO₄)₂, M = Ca, Cu, etc.) in which uranium is incorporated in the form of water-soluble uranyl (UO₂²⁺) salts. Therefore, understanding the physico-chemical interactions of uranyl with the minerals and biological materials contained in the soils is an important issue [2-5]. Among the latter, siderophores occupy a prominent position [6-11]. These natural chelators are low molecular weight compounds that are produced and excreted by microorganisms in order to capture Fe³⁺ from insoluble iron oxo-hydroxides present in the pedological layer [12-14]. Fe³⁺ being hexacoordinate, most siderophores incorporate three bidentate chelating units, which are often derived from hydroxamic acids. The latter coordinate metal cations in the deprotonated, hydroxamate form, as oxygen-based (O,O)⁻ anionic chelates. The simple hydroxamic acids NMAH and PIPOH (Fig. 1) have been used as pertinent models of the linear and cyclic hydroxamic acid subunits incorporated into siderophores [15-17]. In addition to these low molecular weight compounds, more complex aquatic humic substances, which derive from the natural transformation of lignin, have been recognized as responsible for the bioavailability of Fe³⁺ in seawater [18,19]. It was proposed that, as siderophores, humic substances could complex Fe³⁺ thanks to hydroxamate residues [20]. As a matter of fact, simple benzohydroxamic acids were recently used as model compounds for humic substances, able to supply iron to algae [21].

The hypothesis that hydroxamic acid-containing natural compounds could be involved in the complexation of uranyl relies on the similarity of the electronic properties of Fe³⁺ and UO₂²⁺, which are both Lewis acidic cations [22]. In order to get further insight into this important issue, we compare in this paper the binding properties towards uranyl of a primary hydroxamic acid, namely benzohydroxamic acid (BHAH) taken as a model of aquatic humic substances, with those of *N*-methylacetohydroxamic acid (NMAH) [15,22] and 1-hydroxypiperidine-2-one (PIPOH) [16,17] (Fig. 1), both in the gas phase as well as in aqueous solution. These two

secondary hydroxamic acids of linear (NAMH) and cyclic (PIPOH) structures can be considered as models for the binding groups incorporated in many siderophores, such as those of the desferrioxamine and exochelin groups, respectively.

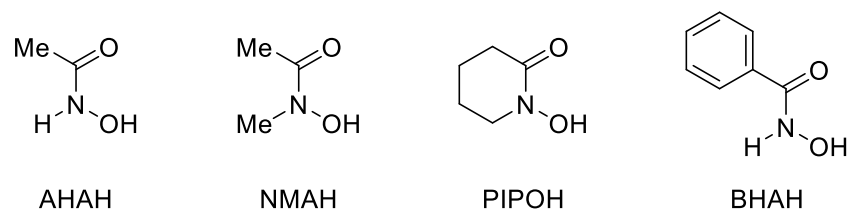


Fig. 1 Molecular formulae (*cis* isomer) and acronym of monohydroxamic acids discussed herein.

Experimental

The detailed description of the synthesis and characterization of the isolated $[\text{UO}_2(\text{BHA})_2(\text{H}_2\text{O})] \cdot 0.85\text{H}_2\text{O}$, $[\text{UO}_2(\text{PIPO})_2(\text{H}_2\text{O})]$ and $[\text{U}^{18}\text{O}_2(\text{PIPO})_2(\text{H}_2\text{O})]$ complexes together with the instrumental methods employed (FT-MIR, Raman, and UV–vis diffuse reflectance spectrophotometry; TGA; (+)-HR-ESI-MS; affinity capillary electrophoresis) is available as Supplementary Information. All errors reported under parentheses correspond to the standard deviation (1σ) rounded to one significant digit.

Results and discussion

Synthesis and characterization of the bischelated uranyl complexes

Treatment of a slight excess (2.5–3 equiv.) of hydroxamic acid dissolved in water with $[\text{UO}_2(\text{NO}_3)_2(\text{H}_2\text{O})_2] \cdot 4\text{H}_2\text{O}$ immediately affords an orange solution, suggesting the formation of complexes that concomitantly lowers the pH to about 2.2. Upon neutralization with an aqueous base solution (~ 0.1 M $\text{N}(\text{CH}_3)_4\text{OH}$ or KOH), a red-orange precipitate corresponding to the neutral bischelated complexes $[\text{UO}_2(\text{L})_2(\text{H}_2\text{O})] \cdot x\text{H}_2\text{O}$ ($x = 1$ for $\text{L} = \text{BHA}^-$, $x = 0$ for $\text{L} = \text{PIPO}^-$) could be isolated in good yield (60–90 %). Both synthesized compounds gave satisfactory elemental analysis and were further characterized by TGA (Fig. S1–S2), IR, Raman, and UV–vis diffuse reflectance spectroscopy in the solid state, and by HR-ESI-MS spectroscopy in solution. Details can be found in the experimental section included in the Supplementary Information.

Vibrational spectroscopy (MIR and Raman) provides a convenient mean to probe the chemical environment of the uranyl cation in its equatorial plane [23,15,17]. Indeed, both the symmetric (ν_s) and antisymmetric (ν_{as}) U=O stretching modes, respectively Raman and IR active, are significantly red-shifted upon chelation with hydroxamate ligands with respect to crystalline $[\text{UO}_2(\text{NO}_3)_2(\text{H}_2\text{O})_2]\cdot 4\text{H}_2\text{O}$ ($\nu_s = 869 \text{ cm}^{-1}$ and $\nu_{as} = 941 \text{ cm}^{-1}$). Both complexes give rise to strong IR absorptions at 906 cm^{-1} , while the Raman shift occurs at 830 cm^{-1} for $[\text{UO}_2(\text{BHA})_2(\text{H}_2\text{O})]\cdot 0.85\text{H}_2\text{O}$ and 835 cm^{-1} in the case of $[\text{UO}_2(\text{PIPO})_2(\text{H}_2\text{O})]$, as typically observed for dihydroxamato uranyl complexes [15,24-26]. A broad feature around 3200 cm^{-1} also attests to the presence of water.

Diffuse reflectance spectra of genuine powdered samples show in the UV range a broad feature corresponding likely to ligand-centered $\pi \rightarrow \pi^*$ transitions at 252 nm in the case of $[\text{UO}_2(\text{PIPO})_2(\text{H}_2\text{O})]$ or at 274 nm in the case of $[\text{UO}_2(\text{BHA})_2(\text{H}_2\text{O})]\cdot 0.85\text{H}_2\text{O}$. In the visible range, two broad and unstructured bands can be assigned to LMCT transitions from the filled π to the empty uranium-centered 5f orbitals [26]. Microcrystalline $[\text{UO}_2(\text{PIPO})_2(\text{H}_2\text{O})]$ gives rise to two well-defined maxima at 386 and 501 nm, while both bands of $[\text{UO}_2(\text{BHA})_2(\text{H}_2\text{O})]\cdot 0.85\text{H}_2\text{O}$ overlap to such an extent that only shoulders are visible around 350 and 470 nm. These characteristics are close to those reported for the red-colored $\{[\text{UO}_2(\text{FHA})_2]\}_n$ coordination polymer formed with formohydroxamate ($\lambda_{\text{max}} = 370$ (sh) and 475 nm) [26]. Noteworthy, both LMCT band maxima of $[\text{UO}_2(\text{PIPO})_2(\text{H}_2\text{O})]$ undergo hypsochromic shifts upon dissolution of the complex in methanol ($\lambda_{\text{max}} = 369$ and 474 nm), whereas slight bathochromic shifts are observed for a methanolic solution of $[\text{UO}_2(\text{BHA})_2(\text{H}_2\text{O})]\cdot 0.85\text{H}_2\text{O}$ ($\lambda_{\text{max}} \approx 360$ and ≈ 460 nm). It can therefore be concluded that some structural rearrangements and/or partial dissociation of the complexes occur in solution. In the crystal state, we have recently shown that $[\text{UO}_2(\text{PIPO})_2(\text{H}_2\text{O})]$ molecules assemble into a head-to-head chain oriented along the x direction through hydrogen bonds involving the protons of the bound water molecule and both hydroxamic O_N atoms from the adjacent motif [17]. Disruption of these H-bonds by methanol might likely affect the coordination sphere around UO_2^{2+} and thus the electronic properties. Although no X-ray quality crystals of $[\text{UO}_2(\text{BHA})_2(\text{H}_2\text{O})]$ could be grown, it can be reasonably assumed that the isolated material has also a polymeric structure, like other uranyl complexes incorporating the primary formo- [26], aceto- [27], or salicylhydroxamate chelates [28]. This assumption is further supported by the very low solubility in water and methanol. If so, slight modifications of the uranyl chromophore

can be expected upon solubilizing the solid material, which should be reflected by shifts of the charge-transfer bands.

Gas phase properties of the bischelated uranyl complexes

Only sparingly soluble in pure methanol, the neutral $[\text{UO}_2(\text{BHA})_2(\text{H}_2\text{O})]\cdot 0.85\text{H}_2\text{O}$ complex readily dissolved upon addition of 15% v/v of DMSO. Thus, a 0.5 mM methanolic solution containing 0.2 mM of DMSO was analyzed by (+)-HR-ESI-MS (Fig. S3). Simulation of the isotopic patterns allowed us to assign without ambiguity all major manifolds appearing in the spectrum. Electrospray ionization generates a variety of solvated monochelated species at $m/z = 484.095$ $[\text{UO}_2(\text{BHA})(\text{DMSO})]^+$, 502.105 $[\text{UO}_2(\text{BHA})(\text{DMSO})(\text{H}_2\text{O})]^+$, 516.121 $[\text{UO}_2(\text{BHA})(\text{DMSO})(\text{CH}_3\text{OH})]^+$, 562.109 $[\text{UO}_2(\text{BHA})(\text{DMSO})_2]^+$, in addition to the bischelated sodium adduct $[\text{UO}_2(\text{BHA})_2(\text{DMSO}) + \text{Na}]^+$ at $m/z = 643.124$, supporting the identity of the isolated complex. MS/MS collision induced dissociation (CID) experiments performed on all of the aforementioned mass-selected cations showed the progressive loss of the various solvent molecules with increasing collision energy (Fig. S4).

These results are in marked contrast with the gas-phase behavior of $[\text{UO}_2(\text{PIPO})_2(\text{H}_2\text{O})]$. Indeed, the MS spectrum of a pure methanolic solution of this compound shows the formation of different monocationic complexes of general $[\text{UO}_2(\text{PIPO})(\text{L})_n]^+$ formula, with L = PIPOH, H_2O , or CH_3OH , in addition to some sodium adducts (see the experimental section in the SI). To get further insight, some mass-selected cations were subjected to CID experiments. MS/MS fragmentation of $[\text{UO}_2(\text{PIPO})(\text{PIPOH})]^+$ ($m/z = 499.161$) affords the $[\text{UO}_2(\text{PIPO})]^+$ cation ($m/z = 384.098$) together with its water adduct ($m/z = 402.104$). CID of the $[\text{UO}_2(\text{PIPO})(\text{PIPOH})_2]^+$ cation ($m/z = 614.225$) gives rise to a new signal at $m/z = 499.156$ associated to the loss of an intact molecule of bound PIPOH ligand (Fig. S5). The thereby generated $[\text{UO}_2(\text{PIPO})(\text{PIPOH})]^+$ cation can further react in the collision chamber with a molecule of water, producing the $[\text{UO}_2(\text{PIPO})(\text{PIPOH})(\text{H}_2\text{O})]^+$ ion detected at $m/z = 517.167$. More intriguingly, CID of $[\text{UO}_2(\text{PIPO})(\text{PIPOH})_2]^+$ generates another peak at $m/z = 596.209$. Accordingly, the lost fragment has a mass of 18.016 a.m.u., suggesting the release of a molecule of water albeit the parent cation is not hydrated. Hence, the abstracted oxygen atom found in the eliminated water molecule can originate either from one hydroxamic ligand or from the UO_2^{2+} cation upon $\text{U}=\text{O}$ bond cleavage. In order to check the latter possibility and to discard the former, we prepared and analyzed likewise the ^{18}O -labelled complex $[\text{U}^{18}\text{O}_2(\text{PIPO})_2(\text{H}_2\text{O})]$

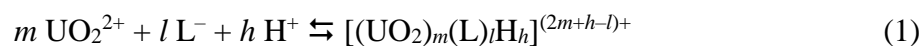
obtained by reacting $U^{18}O_2^{2+}$ with PIPOH (Fig. S6). As expected, the signal assigned to $[U^{18}O_2(PIPO)(PIPOH)_2]^+$ was shifted by 4 mass units with respect to the unlabeled complex ($m/z = 618.227$), while CID unambiguously revealed the elimination of a fragment of 20.014 a.m.u. corresponding to $H_2^{18}O$. This observation clearly ascertains that one "yl" oxygen atom from the UO_2^{2+} core was abstracted, suggesting that one U=O bond is broken during the collision process. This experiment definitively rules out the second conceivable water-elimination mechanism, whereby the oxygen atom would have originated from one coordinated ligand upon N–O or C–O bond cleavage.

Thus far, CID induced U=O bond activation has only rarely been reported in the literature [29-32], although Terencio et al. described very recently a similar situation for the related $[UO_2(NMA)(NMAH)_2]^+$ gas-phase complex [22]. Probed by infrared multiphoton dissociation spectroscopy (IRMPD) and DFT calculations, the most stable and thus plausible structure of that cation revealed the presence of only four oxygen atoms in the equatorial plane of the bound uranium center, two of them being provided by a bischelated NMA^- ligand, while the two remaining ones are provided by carbonyl groups of the monodentate NMAH moieties. One N–OH function was found interacting with one "yl" oxygen atom and the second hydroxyl group was also hydrogen bonded to the former N–OH oxygen atom. Evidence for U=O bond activation was clearly provided by the disappearance of the characteristic antisymmetric O=U=O stretching mode at $\sim 940\text{ cm}^{-1}$ in the IRMPD spectrum of the dehydrated species, which therefore incorporates an UO^{4+} core. Water elimination appeared to be favored by the direct apical $U=O\cdots HO-N$ hydrogen bond that weakens the U=O bond and by the nearby location of a second hydroxyl proton [32,33]. Interestingly, neither the dehydrated $[UO(NMA)_3]^+$ nor $[UO(PIPO)_3]^+$ cation underwent further dissociation or bond activation upon increasing the collision energy. The reason why $[UO_2(BHA)_2(H_2O)]$ behaves markedly differently from $[UO_2(PIPO)_2(H_2O)]$ or $[UO_2(NMA)_2(H_2O)]$ in an ESI source is not fully clear at that point.

Affinity capillary electrophoresis (ACE)

Uranyl complex formation equilibria with benzohydroxamic acid have been investigated at constant ionic strength ($I = 0.1\text{ M (H,Na)ClO}_4$), pH (2.00(5) and 2.50(5)), and temperature ($T = 298(1)\text{ K}$) by affinity capillary electrophoresis (ACE) in aqueous media. This speciation technique relies on the changes of the electrophoretic mobility of the detected species that is produced by the interaction with substrates present in the background electrolytes (BGE) [34-

37]. Recently, ACE has been successfully used for measuring uranyl binding constants with both organic and inorganic ligands in aqueous solution [38-40,17,41]. Global stability constants β_{mlh} associated to equilibrium (1) are defined as molar concentration ratios according to Eq. (2), in which L^- stands for the deprotonated ligand, while charges are omitted for sake of clarity.



$$\beta_{mlh} = \frac{[(\text{UO}_2)_m(\text{L})_l\text{H}_h]}{[\text{UO}_2]^m [\text{L}]^l [\text{H}]^h} \quad (2)$$

A UV detector was used to monitor the migration of the uranium(VI) species as a function of the total BHAH concentration present in the BGE. Fig. S7 reproduces experimental electrophoregrams recorded for a total uranyl concentration of 0.1 mM at both considered pH values. Each trace shows a single signal for which the characteristic migration time taken at the peak maximum (t) increases with the total BHAH content. Such a behavior is typically observed for labile systems and reflects fast ligand exchange processes at the separation time scale (~4 min) between the free and bound uranyl species [35,42,43]. At pH 2.50, uranyl migration is slowed down much more than at pH 2.00 for an identical total ligand concentration, suggesting complex formation to a greater extent. Chelation under strongly acidic conditions was further supported by a bathochromic shift of the absorption band, as the free uranyl peak detected at 200 nm progressively vanishes. Hence, the monitoring wavelength, initially set at 200 nm ($[\text{BHAH}]_{\text{tot}} = 0\text{--}2$ mM), was changed first to 230 nm ($[\text{BHAH}]_{\text{tot}} = 5\text{--}20$ mM), and finally to 250 nm for the last run ($[\text{BHAH}]_{\text{tot}} = 50$ mM).

The observed electrophoretic mobility (μ_{obs}) for labile systems is related to the experimental migration time (t) by Eq. (3), in which L_t stands for the total capillary length (m), L_d for the distance between the capillary inlet and the detection window (m), U for the applied voltage (V), and t_{eof} for the migration time of the neutral marker (s). Noteworthy, t_{eof} (9 min 23 s) remained constant within ± 8 s over the entire concentration range, excluding any complications associated with viscosity effects [40,44].

$$\mu_{\text{obs}} = \frac{L_t L_d}{U} \left(\frac{1}{t} - \frac{1}{t_{\text{eof}}} \right) \quad (3)$$

Variations of μ_{obs} with the total amount of ligand introduced in the BGE (Fig. 2) can be modelled by expression (4), in which α_{mlh} corresponds to the molar fraction of any uranyl-containing species and μ_{mlh} to the intrinsic electrophoretic mobility of the pure $[(\text{UO}_2)_m(\text{L})_l\text{H}_h]^{(2m+h-l)+}$ complex. It should be noted that neutral complexes, e.g. $[\text{UO}_2(\text{BHA})_2(\text{H}_2\text{O})]$, do not contribute directly to the overall electrophoretic mobility ($\mu_{mlh} = 0 \text{ m}^2 \text{ V}^{-1} \text{ s}^{-1}$), but only indirectly as their occurrence impacts the molar fractions of the other charged species.

$$\mu_{\text{obs}} = \sum \alpha_{mlh} \mu_{mlh} \quad (4)$$

Under our acidic conditions, uranium(VI) prevails in the form of the pentaquo uranyl dication. According to the overall equilibrium (1), progressive chelation of $[\text{UO}_2(\text{H}_2\text{O})_5]^{2+}$ by the hydroxamate anionic ligand lowers the overall charge and simultaneously increases the hydrodynamic radius. Both effects are responsible for reducing the apparent electrophoretic mobility (Fig. 2), as reflected by longer migration times. Nonlinear least-squares fit (NLLS) of the experimental μ_{obs} values obtained at different total ligand concentrations, was performed for three chemical models including the formation of either the sole monochelate $[\text{UO}_2(\text{BHA})(\text{H}_2\text{O})_3]^+$ (β_{110} , model 1:1), the sole neutral bischelate $[\text{UO}_2(\text{BHA})_2(\text{H}_2\text{O})]$ (β_{120} , model 1:2), or both complexes (β_{110} and β_{120} , model 1:1 & 1:2).

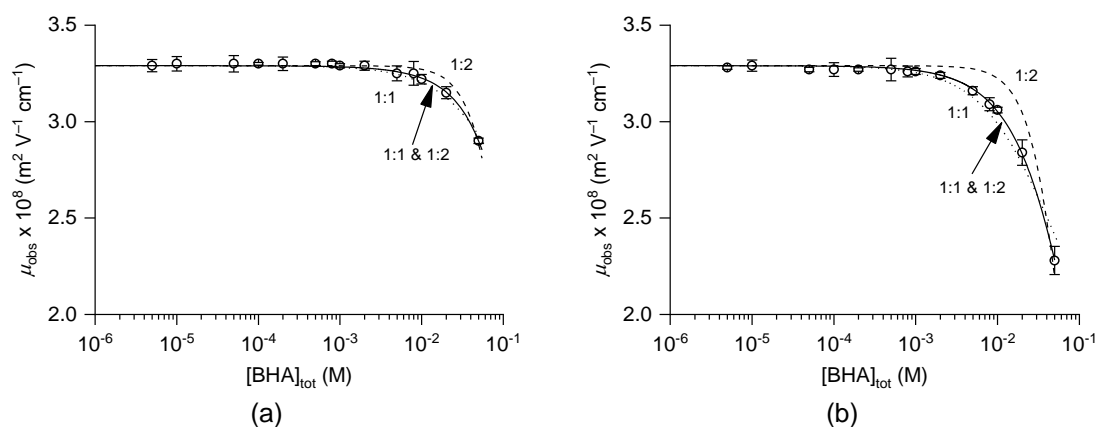


Fig. 2 Variations of the observed electrophoretic mobility of uranyl as a function of the total BHAH concentration at pH = 2.00(5) (a) and 2.50(5) (b). $I = 0.1 \text{ M (H,Na)ClO}_4$, $T = 298(1) \text{ K}$, $[\text{U(VI)}]_{\text{tot}} = 0.1 \text{ mM}$. The solid lines correspond to the best fit obtained for the model 1:1 & 1:2 with $\mu_{110} = 1.4 \times 10^{-8} \text{ m}^2 \text{ V}^{-1} \text{ s}^{-1}$ taken as fixed value. The calculated curves for the 1:1 and 1:2 models are drawn as dotted and dashed lines, respectively. Error bars correspond to the confidence interval at the 95% probability level of the average mobility calculated for three replicates ($\pm t\sigma/\sqrt{n}$).

Since Eq. (4) is homogeneous to the expression of the NMR chemical shift for a given spin system present in several species in fast exchange, ACE data can be advantageously processed with the HypNMR program [45]. This software solves the mass-balance equations for all data points at each NLLS cycle and thus allows refining both the equilibrium constants and the intrinsic electrophoretic mobilities (μ_{mlh}). Because $[\text{UO}_2(\text{BHA})_2(\text{H}_2\text{O})]$ is a neutral species, μ_{120} was set at zero. Likewise, the protonation constant of BHA^- was fixed to the value taken from the literature at the same temperature and ionic strength ($\log K_{011} = 8.80$; selected data are collected in Table S1). Nevertheless, the refinement failed to converge when the β_{110} and μ_{110} were allowed to vary simultaneously, as a consequence of the rather flat error hypersurface in the μ_{110} direction. In other words, the system suffers from a mathematical indetermination, meaning that the product $\alpha_{110}\mu_{110}$ is well defined but each individual term cannot be precisely determined. This behavior is a direct consequence of the non-sigmoidal shape of both curves shown in Fig. 2, suggesting that the complex formation is far from being complete. To reach convergence, it was therefore necessary to make a reasonable guess of the μ_{110} value and keep it constant. As a first approximation, the mobility of $[\text{UO}_2(\text{BHA})(\text{H}_2\text{O})_3]^+$ was assumed to be close to the experimental value determined for the related complex $[\text{UO}_2(\text{PIPO})(\text{H}_2\text{O})_3]^+$ ($\mu_{110} = 1.44(6) \times 10^{-8} \text{ m}^2 \text{ V}^{-1} \text{ s}^{-1}$) [17], implicitly suggesting that the Stokes radii of both monovalent cations are similar. Considering the hydrophobicity of the phenyl substituent attached to the carbonyl group of BHAH and its larger size when compared to the cyclohexyl ring of PIPOH, it might be anticipated that the radius of $[\text{UO}_2(\text{BHA})(\text{H}_2\text{O})_3]^+$ is somewhat larger than that of

the model complex $[\text{UO}_2(\text{PIPO})(\text{H}_2\text{O})_3]^+$, and consequently μ_{110} should be slightly lower. We therefore set μ_{110} at $1.4 \times 10^{-8} \text{ m}^2 \text{ V}^{-1} \text{ s}^{-1}$, which can be considered as an upper limit. In turn, the well-defined plateau seen in Fig. 2 at low total BHAH concentrations enabled us to calculate a reliable estimate for the mobility of free uranyl. The best-fit value ($\mu_{100} = 3.295(3) \times 10^{-8} \text{ m}^2 \text{ V}^{-1} \text{ s}^{-1}$) found for model 1:1 & 1:2 (*vide infra*) is in excellent accordance with the mean value determined in the absence of ligand at both pH's ($\mu_{100} = 3.287(8) \times 10^{-8} \text{ m}^2 \text{ V}^{-1} \text{ s}^{-1}$).

Under such conditions, model 1:2 gave the poorest fit at any pH value and had to be discarded, while model 1:1 did not reproduce well all the data points, especially those measured at pH 2.50 for the highest ligand concentrations. The goodness-of-fit, assessed by the overall standard deviation returned by the software and by the visual inspection of the residues, significantly improved when the three species model 1:1 & 1:2 was considered. Best estimates of the overall stability constants defined by Eq. (2) were obtained after merging all data points recorded at pH 2.00 and 2.50. Refined values are $\log \beta_{110} = 7.43(2)$ and $\log \beta_{120} = 14.47(4)$. Accordingly, the stepwise stability constant of $[\text{UO}_2(\text{BHA})_2(\text{H}_2\text{O})]$, expressed as $\log K_{120} = \log \beta_{120} - \log \beta_{110}$, equals 7.04(6).

Since the mobility of $[\text{UO}_2(\text{BHA})(\text{H}_2\text{O})_3]^+$ is not known precisely, a sensitivity study was performed by assuming an uncertainty on μ_{110} of ca. 25% or $\pm 0.4 \times 10^{-8} \text{ m}^2 \text{ V}^{-1} \text{ s}^{-1}$ [46]. When μ_{110} was set at the lower boundary value of $1.0 \times 10^{-8} \text{ m}^2 \text{ V}^{-1} \text{ s}^{-1}$, the returned equilibrium constants were lowered by 0.08 and 0.15 log units, respectively, as the refinement converged for $\log \beta_{110} = 7.35(2)$ and $\log \beta_{120} = 14.32(6)$, while the overall standard deviation of the fit increased by ca. 4.5%. For $\mu_{110} = 1.8 \times 10^{-8} \text{ m}^2 \text{ V}^{-1} \text{ s}^{-1}$, a less likely situation as stressed above, the program returned higher β_{110} values ($\log \beta_{110} = 7.53(2)$, $\log \beta_{120} = 14.62(3)$). As a matter of fact, the confidence interval on both stepwise binding constants has to be enlarged by about ± 0.1 log unit and the proposed values are $\log K_{110} = 7.4(1)$ and $\log K_{120} = 7.0(1)$. Accordingly, the molar fraction of $[\text{UO}_2(\text{BHA})(\text{H}_2\text{O})_3]^+$ reaches 17 and 36% at pH 2.00 and 2.50, respectively, at the highest total ligand concentration used herein (50 mM). In turn, only 10% of the total uranium occurs as the neutral bischelated complex at pH 2.50, which is within the threshold range for defining a minor species. At pH 2.00, α_{120} is less than 2%, in agreement with the experimental finding that $[\text{UO}_2(\text{BHA})_2(\text{H}_2\text{O})]$ does not contribute to the overall electrophoretic mobility. Based on that, the $\log K_{120}$ value should be considered as less reliable than $\log K_{110}$, and its uncertainty range is probably larger than ± 0.1 .

Table 1 Literature survey of the stability constants for the uranyl/benzohydroxamate (BHA⁻) system

log K_{110}	log K_{120}	I (M)	Medium	T (K)	Method ^a	Ref
7.51(5)	7.1(1)	→0 ^b	NaClO ₄	295.2	UV–vis	[47]
7.5(1)	8.7(5)	→0 ^b	NaClO ₄	298.2	TRLFS	[48]
7.8(2)	7.2(2)	→0 ^b	(H,Na)ClO ₄	298(1)	ACE	This work
8.72	8.05	Variable	KClO ₄	298.2	Pot.	[49]
7.96(5)	7.3(1)	0.1	NaClO ₄	295.2	UV–vis	[47]
7.9(1)	9.0(5)	0.1	NaClO ₄	298.2	TRLFS	[48]
7.4(1)	7.0(1)	0.1	(H,Na)ClO ₄	298(1)	ACE	This work
9.03	8.91	0.1	NaClO ₄	303.2	Pot.	[50]
7.42(1)	6.77(1)	0.1	NaNO ₃	298.2	Pot.	[51]
7.42(3)	6.70(1)	0.1	NaNO ₃	298.2	Pot.	[52]
7.49(3)	6.68(8)	0.1	KNO ₃	298.2	Pot.	[53]
7.7		1.0	NaClO ₄	293.2	UV–vis	[54]

^a Method used: absorption spectrophotometry (UV–vis), affinity capillary electrophoresis (ACE), glass-electrode potentiometry (Pot.), time-resolved laser-induced fluorescence spectroscopy (TRLFS).

^b Extrapolation to $I = 0$ using the Davies equation (Eq. (5)).

Values of the stepwise equilibrium constants (K_{mlh}) determined in this work for the UO₂²⁺/BHA⁻ system are compared in Table 1 to those reported in the literature. Most data were determined by glass-electrode potentiometry, although some authors used UV–vis absorption spectrophotometry or time-resolved laser fluorescence spectroscopy (TRLFS), but ACE has never been applied until now. Examination of Table 1 reveals three potentiometric studies carried out in nitrate media at the same temperature (298.2 K) and ionic strength ($I = 0.1$ M) as our work, which propose remarkably consistent values for log K_{110} and log K_{120} , averaging 7.44(4) and 6.72(5), respectively [51-53]. Noteworthy, the log K_{110} value determined herein by ACE is in excellent accordance with those of references [51-53], while our log K_{120} is slightly higher by ca. 0.3 units.

In contrast, the equilibrium constants determined at 303.2 K by Dutt and Seshari [50] appear as outliers, as they exceed by more than 1.5 orders of magnitude the latter data. It can also be noted that log $K_{120} = 8.91$ almost equals log $K_{110} = 9.03$, which would suggest a cooperative uptake of the second monohydroxamate ligand, a quite unlikely situation for this class of ligands [55,56]. Indeed, the lower probability for the second compared to the first entering bidentate chelator to find an unoccupied binding position in the equatorial plane of a pentacoordinated

uranium center decreases K_{120} with respect to K_{110} . Based on that sole statistical effect, both constants should be in the 1/5 ratio, translating into a $\Delta_{1,2}$ difference ($\Delta_{1,2} = \log K_{110} - \log K_{120}$) of 0.70 units or $\Delta\Delta G_{\text{stat}} = 4.0 \text{ kJ mol}^{-1}$ [17]. In addition, the lower electrostatic interaction energy resulting from the overall charge reduction on the metal center upon progressive uptake of anionic ligands should further lower the binding affinity for the second hydroxamate anion and thus $\Delta_{1,2}$ values even larger than 0.70 are anticipated [17]. Based on that reasoning, the results of Dutt and Seshari [50] but also those of Glorius *et al.* obtained by TRLSF [48] can be considered as suspicious. The spectrophotometric measurements undertaken by the same authors [47] returned apparently more reasonable binding constants, although K_{110} and K_{120} are ca. 0.5 and 0.3 log units higher than our values, respectively. Nevertheless, charge reduction occurs upon successive chelation of UO_2^{2+} by BHA^- . Thus, stability constants at infinite dilution (K_{110}^0) are predicted to be higher than those determined at the ionic strength conditions listed in Table 1. Extrapolation of K_{110} values to $I = 0$ can be achieved in first approximation by applying the Davies equation (Eq. (5) with $\Delta z^2 = -4$ and -2 for $l = 1$ and 2 , respectively) for estimating the activity coefficients of the charged species [57]. By doing so, Glorius *et al.* seemingly calculated K_{110}^0 values lower than those measured at $I = 0.1 \text{ M}$ both by absorption and emission spectrophotometry [47]. If it is assumed that this obvious inconsistency is due to the accidental reversing of K_{110} and K_{120}^0 by the authors in both of their publications, then a good agreement can be found for their values determined by spectrophotometry [47] with those reported herein or in references [51-53].

$$\log K_{110}^0 = \log K_{110} - 0.509\Delta z^2 \left(\frac{\sqrt{I}}{1 + \sqrt{I}} - 0.3I \right) \quad (5)$$

The binding affinity of BHA^- for UO_2^{2+} found herein is significantly lower than that reported at the same temperature and ionic strength for acetohydroxamate (AHA^- , $\log K_{110} = 8.22$, $\log K_{120} = 7.08$) [58], in agreement with the higher basicity of the latter ligand ($\log K_{011} = 9.30(4)$ [56,58] vs. 8.80 at $I = 0.1 \text{ M}$). In turn, the secondary hydroxamate NMA^- possesses a markedly lower basicity ($\log K_{011} = 8.68(3)$, $I = 0.1 \text{ M}$, $T = 298.2 \text{ K}$ [17]) than AHA^- , owing to the stabilization of the positive charge appearing on the nitrogen atom in the iminium canonical form, but is only very slightly more acidic (by ca. 0.1 log unit) than BHA^- . Nevertheless, NMA^- forms a moderately stronger 1:1 complex with uranyl ($\log K_{110} = 7.76(1)$) than BHA^- under similar conditions, while the reverse situation was found in the case of the 1:2 species ($\log K_{120} = 6.14(1)$ for NMA^-) [17]. Very recently, we have investigated the speciation of the UO_2^{2+} in

the presence of the six-membered cyclic hydroxamate PIPO⁻ by combining potentiometric, UV-vis, ACE, and Raman equilibrium measurements [17]. This chelator assumes by construction a blocked *cis* orientation of both donor atoms, unlike the open-chain hydroxamates, which are prone to occur in solution as a mixture of both *cis* and *trans* rotamers (Fig. 1) [15,59,60]. The *cis* conformation of PIPO⁻ confers a higher basicity ($\log K_{011} = 8.85(2)$) and affinity towards UO₂²⁺ ($\log K_{110} = 8.58(1)$, $\log K_{120} = 6.92(1)$, $I = 0.1$ M, $T = 298.2$ K) as compared to NMA⁻, the stability gain amounting 0.8 log units or 4.6 kJ mol⁻¹ per bound ligand. Interestingly, BHA⁻, which exhibits acid-base properties very similar to those of PIPO⁻ and which prevails in water in its *cis* form [59], forms significantly weaker ML ($\log K_{110} = 7.44(4)$ vs. 8.58(1)) and ML₂ ($\log K_{120} = 6.72(5)$ vs. 6.92(1)) complexes with uranyl, highlighting the advantage of a sterically constrained and predisposed structure over an acyclic one. A better solvation by the water molecules of the aliphatic PIPO⁻-complexes might also contribute to enhance their stability.

Conclusions

This study has focused on BHAH, a hydroxamic acid carrying an aromatic carbonyl substituent. Whereas this structural feature has virtually no influence on the p*K*_a of BHAH by comparison with aliphatic analogues (NMAH and PIPOH), the binding properties of BHA⁻ towards the uranyl dication are affected to a significant extent, since they can be viewed as intermediate between those of NMA⁻ and PIPO⁻. The affinity of UO₂²⁺ for a first BHA⁻ ligand is very similar to that for NMA⁻, whereas the second BHA⁻ chelate is captured with the same affinity as PIPO⁻. Overall, however, BHA⁻ behaves as a standard hydroxamate as far as the complexation of UO₂²⁺ in aqueous solution is concerned. The situation is more contrasted in the gas phase. The collision-induced U=O bond cleavage phenomenon observed in the case of the [UO₂(NMA)(NMAH)₂]⁺ species, and reported in an earlier work, could be duplicated with the PIPOH ligand, but not with BHAH. In the latter case, the more classical release of a BHA⁻ chelate was observed instead. Whereas gas phase studies are a direct entry into bond energetics, fundamental solution studies allow us to understand and describe phenomena taking place not only *in vitro*, but also *in vivo*. The demonstration that BHA⁻ can complex uranyl as efficiently as aliphatic hydroxamic siderophores makes this chelate a pertinent model of humic substances,

which have been recognized as a class of natural compounds involved in the mobilization of hard Lewis acids such as UO_2^{2+} or Fe^{3+} .

Acknowledgements

The Centre National de la Recherche Scientifique (CNRS), the Conseil Régional de Bourgogne (CRB, program PARI II CDEA), the European Regional Development Fund (FEDER), the program "Défi NEEDS Environnement" (project PiRATE), and the Agence Nationale de la Recherche (ANR project PLUTON, grant N° ANR-17-CE08-0053) are gratefully acknowledged for their financial support. M.H. and P.J. thank the Chinese government and the CRB, respectively, for their PhD fellowships.

References

1. IRSN sheet N° 1 (2018) The extraction of uranium in France: Data and key figures (in French). Available at http://www.irsn.fr/FR/connaissances/Environnement/expertises-locales/sites-miniers-uranium/Documents/irsn_mines-uranium_extraction-uranium_2017.pdf. Accessed April 2018
2. Crançon P, van der Lee J (2003) *Radiochim Acta* 92:673-679
3. Sherman DM, Peacock CL, Hubbard CG (2008) *Geochim Cosmochim Acta* 72:298-310
4. Mishra S, Maity S, Bhalke S, Pandit G, Puranik V, Kushwaha H (2012) *J Radioanal Nucl Chem* 294:97-102
5. Wang Z, Zachara JM, Boily J-F, Xia Y, Resch TC, Moore DA, Liu C (2011) *Geochim Cosmochim Acta* 75:2965-2979
6. Brainard JR, Strietelmeier BA, Smith PH, Langston-Unkefer PJ, Barr ME, Ryan RR (1992) *Radiochim Acta* 58-59:357-364
7. Bouby M, Billard I, MacCordick J, Rossini I (1998) *Radiochim Acta* 80:95-100
8. Renshaw JC, Halliday V, Robson GD, Trinci APJ, Wiebe MG, Livens FR, Collison D, Taylor RJ (2003) *Appl Environ Microbiol* 69:3600-3606
9. Ruggiero CE, Boukhalfa H, Forsythe JH, Lack JG, Hersman LE, Neu MP (2005) *Environ Microbiol* 7:88-97
10. Frazier SW, Kretzschmar R, Kraemer SM (2005) *Environ Sci Technol* 39:5709-5715
11. Wolff-Boenisch D, Traina SJ (2007) *Chem Geol* 242:278-287

12. Albrecht-Gary AM, Crumbliss AL (1998) Coordination Chemistry of Siderophores: Thermodynamics and Kinetics of Iron Chelation and Release. In: Sigel A, Sigel H (eds) Metal Ions in Biological Systems. Iron Transport and Storage in Microorganisms, Plants, and Animals, vol 35. Marcel Dekker, New York, pp 239-327
13. Stintzi A, Raymond KN (2001) Siderophore Chemistry. In: Templeton DE (ed) Molecular and Cellular Iron Transport. Marcel Dekker, New York, pp 273-319
14. Dertz EA, Raymond KN (2004) Biochemical and Physical Properties of Siderophores. In: Crosa JH, Mey AR, Payne S (eds) Iron Transport in Bacteria. ASM Press, Washington, DC, pp 5-17
15. Brandès S, Sornosa-Ten A, Rousselin Y, Lagrelette M, Stern C, Moncomble A, Cornard J-P, Meyer M (2015) *J Inorg Biochem* 151:164-175
16. Jewula P, Berthet J-C, Chambron J-C, Rousselin Y, Thuéry P, Meyer M (2015) *Eur J Inorg Chem*:1529-1541
17. Sornosa-Ten A, Jewula P, Fodor T, Brandes S, Sladkov V, Rousselin Y, Stern C, Chambron J-C, Meyer M (2018) *New J Chem* 42:7765-7779
18. Liu X, Millero FJ (2002) *Mar Chem* 77:43-54
19. Hiemstra T, van Riemsdijk WH (2006) *Mar Chem* 102:181-197
20. Frimmel FH, Geywitz J (1983) *Fresenius' Z Anal Chem* 316:582
21. Orłowska E, Roller A, Wiesinger H, Pignitter M, Jirsa F, Krachler R, Kandioller W, Keppler BK (2016) *RSC Adv* 6:40238-40249
22. Terencio T, Roithová J, Brandès S, Rousselin Y, Penouilh M-J, Meyer M (2018) *Inorg Chem* 57:1125-1135
23. Nakamoto K (1970) *Infrared and Raman Spectra of Inorganic and Coordination Compounds*. Wiley, New York
24. Chakraborty S, Dinda S, Bhattacharyya R, Mukherjee AK (2006) *Z Kristallogr* 221:606-611
25. Hazra DK, Dinda S, Helliwell M, Bhattacharyya R, Mukherjee M (2009) *Z Kristallogr* 224:544-550
26. Silver MA, Dorfner WL, Cary SK, Cross JN, Lin J, Schelter EJ, Albrecht-Schmitt TE (2015) *Inorg Chem* 54:5280-5284
27. Weck PF, Gong C-MS, Kim E, Thuéry P, Czerwinski KR (2011) *Dalton Trans* 40:6007-6011
28. Centore R, De Tommaso G, Iuliano M, Tuzi A (2007) *Acta Crystallogr, Sect C* 63:m253-m255

29. Van Stipdonk MJ, Michelini MdC, Plaviak A, Martin D, Gibson JK (2014) *J Phys Chem A* 118:7838-7846
30. Gong Y, Vallet V, del Carmen Michelini M, Rios D, Gibson JK (2014) *J Phys Chem A* 118:325-330
31. Gong Y, de Jong WA, Gibson JK (2015) *J Am Chem Soc* 137:5911-5915
32. Abergel RJ, de Jong WA, Deblonde GJP, Dau PD, Captain I, Eaton TM, Jian J, van Stipdonk MJ, Martens J, Berden G, Oomens J, Gibson JK (2017) *Inorg Chem* 56:12930-12937
33. Szabó Z, Grenthe I (2007) *Inorg Chem* 46:9372-9378
34. Krylov SN (2007) *Electrophoresis* 28:69-88
35. Jiang C, Armstrong DW (2010) *Electrophoresis* 31:17-27
36. Timerbaev AR, Timerbaev RM (2013) *Trends Anal Chem* 51:44-50
37. Sladkov V (2016) *Electrophoresis* 37:2558-2566
38. Sladkov V (2010) *Electrophoresis* 31:3482-3491
39. Sladkov V (2013) *J Chromatogr A* 1276:120-125
40. Sladkov V (2014) *J Chem Thermodyn* 71:148-154
41. Sladkov V, Bessonov AA, Roques J, Charushnikova IA, Fedosseev AM (2018) *New J Chem* 42:7780-7788
42. Okhonin V, Berezovski MV, Krylov SN (2010) *J Am Chem Soc* 132:7062-7068
43. Kanoatov M, Cherney LT, Krylov SN (2014) *Anal Chem* 86:1298-1305
44. Sladkov V (2013) *J Chromatogr A* 1289:133-138
45. Frassinetti C, Ghelli S, Gans P, Sabatini A, Moruzzi MS, Vacca A (1995) *Anal Biochem* 231:374-382
46. Topin S, Aupiais J, Baglan N, Vercoouter T, Vitorge P, Moisy P (2009) *Anal Chem* 81:5354-5363
47. Glorius M, Moll H, Bernhard G (2007) *Radiochim Acta* 95:151-157
48. Glorius M, Moll H, Geipel G, Bernhard G (2008) *J Radioanal Nucl Chem* 277:371-377
49. Baroncelli F, Grossi G (1965) *J Inorg Nucl Chem* 27:1085-1092
50. Dutt NK, Seshadri T (1969) *J Inorg Nucl Chem* 31:2153-2157
51. Khairy EM, Shoukry MM, Khalil MM, Mohamed MMA (1996) *Transition Met Chem* 21:176-180
52. Khalil MM, El-Deeb MM, Mahmoud RK (2007) *J Chem Eng Data* 52:1571-1579
53. Koide Y, Uchino M, Shosenji H, Yamada K (1989) *Bull Chem Soc Jpn* 62:3714-3715
54. Maggio F, Romano V, Cefalù R (1966) *J Inorg Nucl Chem* 28:1979-1984

55. Kurzak B, Kozłowski H, Farkas E (1992) *Coord Chem Rev* 114:169-200
56. Farkas E, Kozma E, Petho M, Herlihy KM, Micera G (1998) *Polyhedron* 17:3331-3342
57. Grenthe I, Wanner H, Östhols E (2000) TDB-2 Guidelines for the extrapolation to zero ionic strength. OECD Nuclear Energy Agency, Issy-les-Moulineaux
58. Martell AE, Smith RM, Motekaitis RJ (2004) NIST Critically Selected Stability Constants of Metal Complexes Database. 8.0 edn. NIST Standard Reference Database No. 46, Gaithersburg, MD
59. García B, Ibeas S, Leal JM, Secco F, Venturini M, Senent ML, Niño A, Muñoz C (2005) *Inorg Chem* 44:2908-2919
60. Sippl SP, Schenck HL (2013) *Magn Reson Chem* 51:72-75